








Response of a lead-free borosilicate-glass microchannel plate to 14-MeV neutrons and γ -rays

Cite as: Rev. Sci. Instrum. **90**, 103306 (2019); <https://doi.org/10.1063/1.5109103>

Submitted: 06 May 2019 . Accepted: 25 September 2019 . Published Online: 15 October 2019

C. E. Parker , J. A. Frenje , O. H. W. Siegmund, C. J. Forrest, V. Yu. Glebov, J. D. Kendrick , C. W. Wink , M. Gatu Johnson , T. J. Hilsabeck, S. T. Ivancic, J. Katz, J. D. Kilkenny, B. Lahmann , C. K. Li, F. H. Séguin, C. M. Sorce, C. Trosseille, and R. D. Petraso 



[View Online](#)



[Export Citation](#)



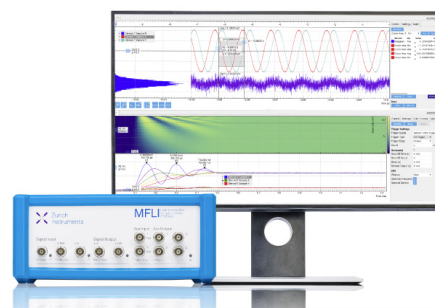
[CrossMark](#)

Challenge us.

What are your needs for periodic signal detection?



Zurich
Instruments



Response of a lead-free borosilicate-glass microchannel plate to 14-MeV neutrons and γ -rays

Cite as: Rev. Sci. Instrum. 90, 103306 (2019); doi: 10.1063/1.5109103

Submitted: 6 May 2019 • Accepted: 25 September 2019 •

Published Online: 15 October 2019



View Online



Export Citation



CrossMark

C. E. Parker,^{1,a)} J. A. Frenje,¹ O. H. W. Siegmund,² C. J. Forrest,³ V. Yu. Glebov,³ J. D. Kendrick,³ C. W. Wink,¹ M. Gatu Johnson,¹ T. J. Hilsabeck,⁴ S. T. Ivancic,³ J. Katz,³ J. D. Kilkenny,⁴ B. Lahmann,¹ C. K. Li,¹ F. H. Séguin,¹ C. M. Sorce,³ C. Trosseille,⁵ and R. D. Petrasso¹

AFFILIATIONS

¹Massachusetts Institute of Technology, Cambridge, Massachusetts 02139, USA

²Space Sciences Laboratory, University of California, Berkeley, California 94720, USA

³Laboratory for Laser Energetics, University of Rochester, Rochester, New York 14623, USA

⁴General Atomics, San Diego, California 92186, USA

⁵Lawrence Livermore National Laboratory, Livermore, California 94550, USA

^{a)}Author to whom correspondence should be addressed: cparker@psfc.mit.edu

ABSTRACT

In microchannel plate applications, such as in space telescopes, night-vision devices, or time-of-flight particle detection, reducing the sensitivity to signals from background sources, such as γ -rays, is beneficial for the system design and performance. The response of a single-stage lead-free borosilicate-glass microchannel plate to 14-MeV neutrons and γ -rays produced via (n, γ) reactions in surrounding structures was investigated at OMEGA. The average efficiency values for secondary electron production were found to be $(5.1 \pm 0.7) \times 10^{-3}$ for 14-MeV neutrons and $(4.9 \pm 1.1) \times 10^{-3}$ for (1.5)-MeV γ -rays.

Published under license by AIP Publishing. <https://doi.org/10.1063/1.5109103>

I. INTRODUCTION AND MOTIVATION

Microchannel plates (MCPs) are used for signal amplification in many detector schemes measuring neutrons, photons, and charged particles across multiple disciplines. Most applications include commercially available lead-glass MCPs of various standard sizes and configurations. However, in some instances, in order to optimize the signal-to-background (S/B) of a system, the proprietary lead-containing glass and standard MCP sizes may not be desirable. One such system currently being designed is the magnetic recoil spectrometer for time-resolved neutron measurements, known as MRSt.^{1–3} This will be the first diagnostic for time-resolved measurements of deuterium-tritium (DT) implosions at the National Ignition Facility (NIF),⁴ from which the evolution of yield, ion temperature (T_{ion}), and areal-density (ρR) can be inferred.

Sources of background that can affect the MRSt are neutrons and γ -rays interacting with the MCP material used for the

amplification of the signal, which for the MRSt are secondary electrons (SE). These SE are produced in a multistep process where neutrons from the implosion impinge upon a CD conversion foil placed on the outside of the *Hohlraum*,⁵ producing elastically scattered deuterons that are momentum analyzed and focused by a magnet system. These deuterons then impinge upon a thin CsI photocathode positioned at the focal plane, producing SE to be amplified by the MCP for the readout in an anode array. The S/B calculations for the preliminary shielding design for the system were based upon previous measurements of the efficiency for generating SE from incoming 14-MeV neutrons⁶ and 1-MeV γ -rays⁷ perpendicularly incident on standard lead-glass MCPs, which were found to be 6.4×10^{-3} and 2.2×10^{-2} , respectively. This produced a S/B value of 6.5 for the region of interest. In addition, the model was applied to lead-free borosilicate glass MCPs, giving a S/B value of 20.7 or a $\sim 3\times$ improvement. For details of the calculations, the reader is referred to Ref. 8.

This paper reports on the first measurement of the response of a lead-free borosilicate glass MCP to 14-MeV neutrons and (1.5)-MeV γ -rays produced in DT implosions at OMEGA.⁹ Section II describes the Monte Carlo N-Particle (MCNP) simulation and the setup for the experiments, including specifications of the MCP detector. Section III discusses the data analysis. Finally, Sec. IV is the conclusion.

II. EXPERIMENTS

The experiments took place at the OMEGA laser facility. The campaign used 880- μm -OD, 4.3- μm -thick Hoppe glass capsules filled with 10 atm of equimolar DT fuel. These were driven with a 1-ns square pulse with ~ 26.5 kJ of laser energy on the target at the Target Chamber Center (TCC), providing average yields of 6.9×10^{13} DT neutrons. The experimental setup, shown in Fig. 1, was located directly below the OMEGA target chamber along the P12 port line-of-sight in LaCave, with the detector face 6.7 m from the TCC.

The MCP detector was fielded inside a lead brick house that was constructed to shield against unwanted scattered neutrons while still leaving an opening for the standalone turbo pump connection as well as the bias and signal cables. The lead bricks were staggered, to avoid the seam being in the same place in each layer, in such a manner that a 2.54-cm by 2.54-cm opening was centered on the face of the MCP detector. This was to allow for a known collimated opening for the incoming neutrons and γ -rays. The configuration was varied by adding an additional lead brick over the collimated opening to investigate the attenuation of the signals, leading to the setup either being fielded with the lead lid “off” or “on.”

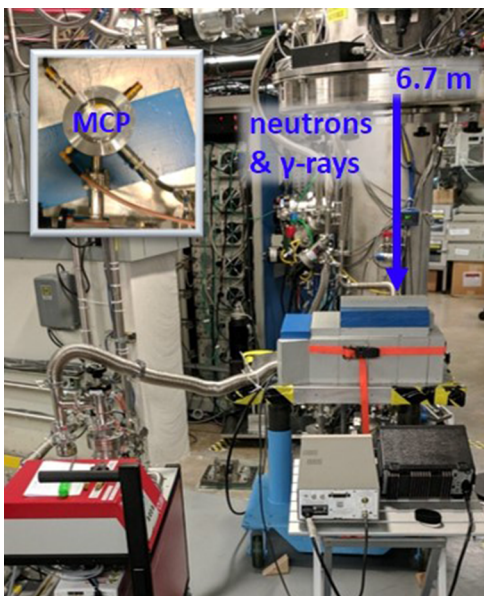


FIG. 1. MCP test setup (with lead lid on) located below the OMEGA target chamber lower pylon; (inset) the demountable MCP detector assembly was fielded inside the lead brick house, perpendicular to the incoming neutrons and γ -rays at 6.7 m from the TCC.

A. MCNP model

Figure 2 shows a portion of the MCNP model of the experiment that was used to simulate the incident number of neutrons and γ -rays incident at the MCP; it is based on the model used for neutron spectroscopy measurements at OMEGA.¹⁰ The model includes the OMEGA and OMEGA-EP target bays, walls, and floors; the aluminum OMEGA target chamber with simplified lower pylon re-entrant tube components; LaCave with the hole in the ceiling and stainless steel cover; and detector setup, including the MCP detector and lead house.

The simulation was run for 5×10^9 incident particles simulating a thermal DT plasma with an apparent ion temperature of 10 keV, which produces 14-MeV neutrons. This was done for both the lid-on and lid-off configurations, with the output shown in Fig. 3. To run the simulation in the lid-off configuration, the lid material was changed from lead to air. For the lid on case vs the lid off case, the expected neutron fluence dropped by $\sim 15\%$, while the expected γ -ray flux dropped by $\sim 30\%$ for the primary peaks centered at ~ 140 ns and ~ 50 ns for neutrons and γ -rays, respectively.

The MCNP simulations were also parsed into 100-keV increments for the energy distribution of γ -rays incident at the MCP detector location as shown in Fig. 4. The weighted-average energy for the γ -rays was found to be (1.5)-MeV based on the simulation for both configurations.

B. Detector and signal processing

The detector consisted of a single MCP manufactured from a borosilicate microcapillary array, with atomic layer deposition (ALD) utilized to tailor the SE emission and resistance properties of the MCP.^{11,12} The 33-mm-diameter MCP had a 20- μm pore size and a 60:1 aspect ratio. Once in the detector housing, along the collimated line-of-sight, the active diameter of the MCP was reduced to ~ 25 mm. The detector housing was kept under a vacuum of $\sim 1.2 \times 10^{-6}$ mbar for the duration of the experiments. Previous characterization of this size of lead-free MCP indicates that the efficiency for SE production due to incoming γ -rays from a ^{60}Co source was reduced by a factor of ~ 2.5 when compared to standard lead-glass.¹³

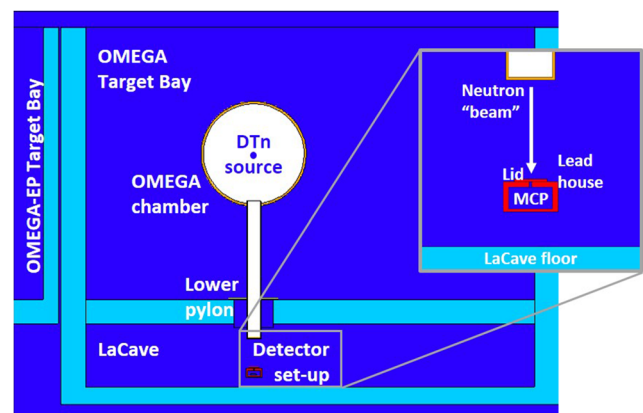


FIG. 2. Vised rendering of the full MCNP setup; inset shows the MCP detector, lead house with collimated opening covered by the lead lid, and the LaCave floor. The MCP detector face was 75.5 cm from the bottom of the lower pylon valve cover.

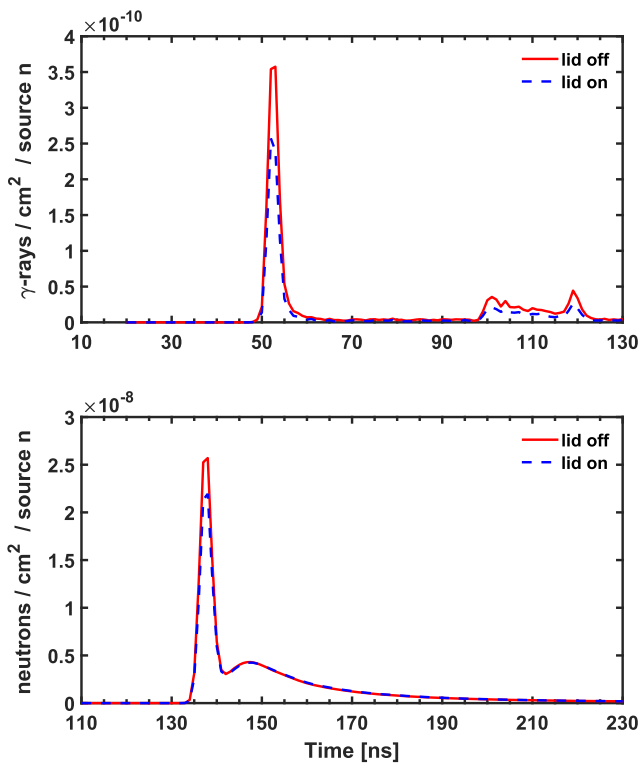


FIG. 3. MCNP time-of-flight output for (upper) γ -rays and (lower) neutrons at the MCP detector location. In each case, the red solid line is the simulation for the lid off configuration; the blue dashed line is for the lid on configuration.

The gain of the single-MCP system was measured by illuminating the MCP with UV light at a sufficiently low level to generate a single photoelectron per laser pulse. A high-speed oscilloscope recorded the output electrical signal from the MCP from triggered single events. Using this process, 1000 such single

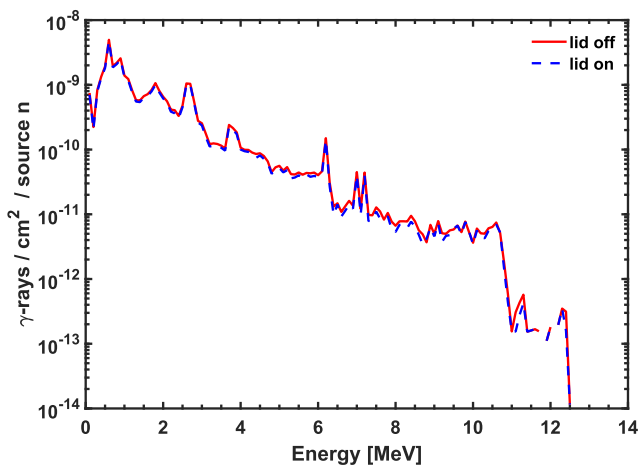


FIG. 4. MCNP output for the γ -ray energy distribution at the MCP detector location. The red solid line is the simulation for the lid off configuration; the blue dashed line is for the lid on configuration.

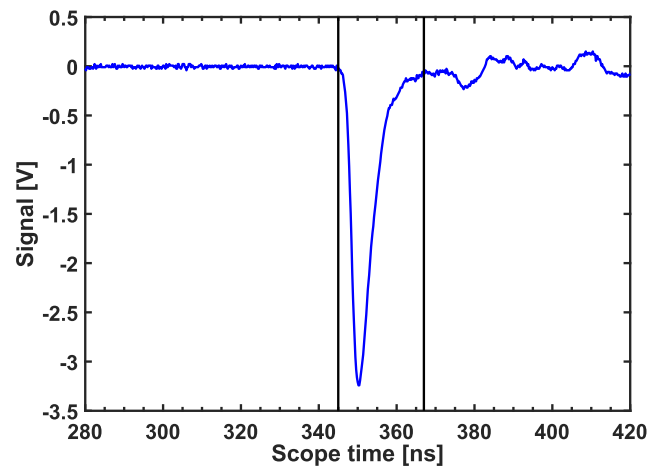


FIG. 5. Scope trace of the 14-MeV neutron signal for shot 85 913. The black vertical lines indicate the region of interest. Features in the waveform after 375 ns are artifacts from ringing in the cabling, not signal.

events were recorded, and the integrated charge from the MCP as a function of voltage was determined; this process was repeated three times. Using this technique, the integrated charge is the gain as the input was a single electron. The measured values are within an order of magnitude of the gains of other MCPs of the same specifications.

The detector was biased using a Stanford Research Systems PS350 adjustable high voltage power supply. Signals from the MCP were collected and processed using the same configuration as an ungated neutron time-of-flight detector.¹⁴ The SubMiniature version A (SMA) signal output was adapted to connect to a N-type LMR-400 cable connected to a 2.5-GHz, 10 Gs/s Tektronix DPO-7204 oscilloscope. The input to the oscilloscope was divided into four channels using a resistive splitter to ensure that the dynamic range of the system was large enough to record the signals.

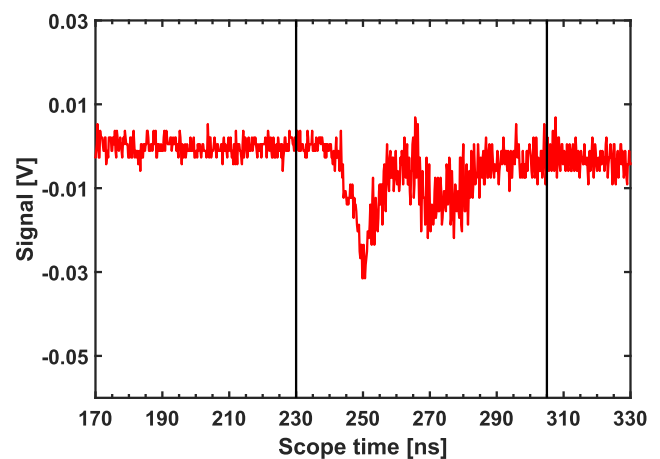


FIG. 6. Scope trace of shot 85 913 γ -rays produced in (n, γ) reactions from interactions with the target chamber and other surrounding materials. The black vertical lines indicate the region of interest.

TABLE I. SE per 14-MeV neutron and SE per (1.5)-MeV γ -ray for a single-stage borosilicate glass MCP. These data were obtained on 4 shots which yielded a good signal. The MCP was biased to -1100 V for each shot. The DT neutron yields are from the copper activation diagnostic.¹⁵ Uncertainty for the calculated SE efficiency values includes uncertainties added in quadrature, described in detail in the text, of 14% for the SE/n and 20% for the SE/ γ -ray.

Shot	DT yield	Lid off/on?	14-MeV neutrons			(1.5)-MeV γ -rays		
			$Q_{meas,n}$ (pC)	$\eta_{MCNP,n}$	SE/n	$Q_{meas,\gamma}$ (pC)	$\eta_{MCNP,\gamma}$	SE/ γ -ray
85 913	$(7.23 \pm 0.36) \times 10^{13}$	Off	437	9.5×10^{-8}	$(5.3 \pm 0.7) \times 10^{-3}$	10.4	1.9×10^{-9}	$(6.3 \pm 1.3) \times 10^{-3}$
85 916	$(6.99 \pm 0.35) \times 10^{13}$	On	336	8.2×10^{-8}	$(4.9 \pm 0.7) \times 10^{-3}$	3.3	1.2×10^{-9}	$(3.3 \pm 0.7) \times 10^{-3}$
85 917	$(6.92 \pm 0.35) \times 10^{13}$	On	335	8.2×10^{-8}	$(4.9 \pm 0.7) \times 10^{-3}$	3.4	1.2×10^{-9}	$(3.4 \pm 0.7) \times 10^{-3}$
85 918	$(6.65 \pm 0.33) \times 10^{13}$	Off	406	9.5×10^{-8}	$(5.3 \pm 0.7) \times 10^{-3}$	9.9	1.9×10^{-9}	$(6.5 \pm 1.3) \times 10^{-3}$

III. RESULTS AND ANALYSIS

Four shots yielded a measurable signal at a -1100 V bias, two with the lead lid on, and two with the lead lid off, for repeatability. Figures 5 and 6 show the scope traces for the neutrons and γ -rays, respectively, for shot 85 913, which was the configuration fielded with the lid off. As shown in the figure, the scope time is in arbitrary time with respect to $t = 0$ for the shot as the scope was not calibrated for this detector and cable combination. However, the 14-MeV neutron signal arrives ~ 100 ns after the γ -ray signal, as expected based on the time-of-flight to the MCP location. The scope traces for both the neutrons and γ -rays were integrated, then converted to charge collected using the resistance and time bins of the scope, taking into account the resistive splitter.

A. SE generation

The number of SE generated per perpendicularly incident 14-MeV neutron (or (1.5)-MeV γ -ray) was determined using the following relation:

$$\frac{SE}{n(\gamma)} = \frac{Q_{meas,n(\gamma)}}{Q_e \times Y_{DT} \times \eta_{MCNP,n(\gamma)} \times A_{MCP} \times g_{MCP}}, \quad (1)$$

where $Q_{meas,n(\gamma)}$ is the collected charge for neutrons (or γ -rays) in pC; Q_e is the electron charge in pC/e⁻; Y_{DT} is the neutron yield from the implosion; $\eta_{MCNP,n(\gamma)}$ is the fluence of incoming neutrons (or γ -rays)/cm²/source neutron at the detector for the lid configuration (guided by the number of time bins of the scope signal); A_{MCP} is the MCP area in cm²; and g_{MCP} is the gain of the MCP. For the fixed MCP area of 5 cm², and the gain determined from the pulsed laser test, 1.5×10^4 , the number of SE/n and SE/ γ -ray for each shot is shown in Table I.

Uncertainty for the calculated SE efficiency values includes uncertainties added in quadrature for the DT neutron yield (5%), MCNP and geometry (10%), MCP gain (8%), and γ -ray waveform S/B (14%); the neutron waveform S/B is considered to be negligible. The difference in uncertainty for the γ -ray and neutron waveform S/B uncertainties is due to the noise level on the scope baseline, which does not affect the much-larger neutron signals. Additionally, the gain for UV, neutrons, and γ -rays should be identical because the measured gain per photoelectron in the MCP is essentially the electrical amplification. There will be a difference in noise because one γ -ray or neutron may generate many SEs per event, albeit with

a correspondingly low cross section. However, each of those SEs will be amplified by the measured gain.

IV. CONCLUSION

The average efficiency values for SE production for a single-stage borosilicate MCP are found to be $(5.1 \pm 0.7) \times 10^{-3}$ and $(4.9 \pm 1.1) \times 10^{-3}$ for 14-MeV neutrons and (1.5)-MeV γ -rays, respectively, for perpendicular incidence. Previous work used a single-stage lead-glass MCP with a 25- μ m pore size and a 80:1 aspect ratio, with a result of 2.2×10^{-2} for the γ -ray efficiency. Therefore, the γ -ray efficiency for the borosilicate MCP is found to be reduced by a factor of ~ 4 . The voltage at which the MCPs were run only allows events generated at the front face of the MCP to produce events large enough to be counted; therefore, it can be assumed that comparing MCPs with different pore sizes and L/D ratios will have a limited effect on the efficiency. The 14-MeV neutron efficiency for the current work was found to be approximately the same as the previous measurement that used a lead-glass Chevron configuration where the efficiency was found to be 6.4×10^{-3} . Additional testing of the lead-free MCPs at different voltages, in both single-stage and Chevron configurations, would also be beneficial for diagnostic development to reduce potential uncertainty from the behavior of the individual MCPs. In conclusion, the current work indicates that the lead-free MCPs will be a better choice for a system measuring the signal in the presence of a large γ -ray background, particularly if the location of the diagnostic cannot accommodate large amounts of shielding materials.

ACKNOWLEDGMENTS

The authors would like to thank A. Martin, M. Romanofsky, R. Bahr, and the OMEGA operations crew for their assistance in carrying out this work. This work was performed under the auspices of the U.S. Department of Energy by the Lawrence Livermore National Laboratory under Contract No. DE-AC52-07NA27344 and the Laboratory for Laser Energetics (LLE) under subcontract Grant No. 416107-G. This report was prepared as an account of work sponsored by an agency of the United States Government. Reference herein to any specific commercial product, process, or service by trade name, trademark, manufacturer, or otherwise does not necessarily constitute or imply its endorsement, recommendation, or favoring by the United States Government or any agency thereof.

The views and opinions of the authors expressed herein do not necessarily state or reflect those of the United States Government or any agency thereof.

REFERENCES

- ¹J. A. Frenje, T. J. Hilsabeck, C. W. Wink, P. Bell, R. Bionta, C. Cerjan, M. Gatu Johnson, J. D. Kilkenny, C. K. Li, F. H. Séguin, and R. D. Petrasso, *Rev. Sci. Instrum.* **87**, 11D806 (2016).
- ²T. J. Hilsabeck, J. A. Frenje, J. D. Hares, and C. W. Wink, *Rev. Sci. Instrum.* **87**, 11D807 (2016).
- ³C. W. Wink, J. A. Frenje, T. J. Hilsabeck, R. Bionta, H. Y. Khater, M. Gatu Johnson, J. D. Kilkenny, C. K. Li, F. H. Séguin, and R. D. Petrasso, *Rev. Sci. Instrum.* **87**, 11D808 (2016).
- ⁴G. H. Miller, E. I. Moses, and C. R. Wuest, *Nucl. Fusion* **44**, S228 (2004).
- ⁵C. E. Parker, J. A. Frenje, M. G. Johnson, D. J. Schlossberg, H. G. Reynolds, L. B. Hopkins, R. Bionta, D. T. Casey, S. J. Felker, T. J. Hilsabeck, J. D. Kilkenny, C. K. Li, A. J. Mackinnon, H. Robey, M. E. Schoff, F. H. Séguin, C. W. Wink, and R. D. Petrasso, *Rev. Sci. Instrum.* **89**, 113508 (2018).
- ⁶S. S. Medley and R. Persing, *Rev. Sci. Instrum.* **52**, 1463 (1981).
- ⁷J. G. Timothy and R. L. Bybee, *Rev. Sci. Instrum.* **50**, 743 (1979).
- ⁸C. W. Wink, M.Sc. thesis, Massachusetts Institute of Technology, Cambridge, MA, 2017.
- ⁹T. Boehly, D. Brown, R. Craxton, R. Keck, J. Knauer, J. Kelly, T. Kessler, S. Kumpan, S. Loucks, S. Letzring, F. Marshall, R. McCrory, S. Morse, W. Seka, J. Soures, and C. Verdon, *Opt. Commun.* **133**, 495 (1997).
- ¹⁰C. J. Forrest, P. B. Radha, V. Y. Glebov, V. N. Goncharov, J. P. Knauer, A. Pruyne, M. Romanofsky, T. C. Sangster, M. J. Shoup, C. Stoeckl, D. T. Casey, M. Gatu-Johnson, and S. Gardner, *Rev. Sci. Instrum.* **83**, 10D919 (2012).
- ¹¹A. U. Mane, Q. Peng, M. J. Wetstein, R. G. Wagner, H. J. Frisch, O. H. W. Siegmund, M. J. Minot, B. W. Adams, M. C. Chollet, and J. W. Elam, *Proc. SPIE* **8031**, 8031 (2011).
- ¹²O. H. W. Siegmund, N. Richner, G. Gunjala, J. B. McPhate, A. S. Tremsin, H. J. Frisch, J. Elam, A. Mane, R. Wagner, C. A. Craven, and M. J. Minot, *Proc. SPIE* **8859**, 8859 (2013).
- ¹³O. H. W. Siegmund, C. Ertley, J. V. Vallerga, E. R. Schindhelm, A. Harwit, B. T. Fleming, K. C. France, J. C. Green, S. R. McCandliss, and W. M. Harris, *Proc. SPIE* **10397**, 1039711 (2017).
- ¹⁴V. Y. Glebov, C. Forrest, J. P. Knauer, A. Pruyne, M. Romanofsky, T. C. Sangster, M. J. Shoup, C. Stoeckl, J. A. Caggiano, M. L. Carman, T. J. Clancy, R. Hatarik, J. McNaney, and N. P. Zaitseva, *Rev. Sci. Instrum.* **83**, 10D309 (2012).
- ¹⁵O. Landoas, V. Yu Glebov, B. Rossé, M. Briat, L. Disdier, T. C. Sangster, T. Duffy, J. G. Marmouget, C. Varignon, X. Ledoux, T. Caillaud, I. Thfoin, and J.-L. Bourgade, *Rev. Sci. Instrum.* **82**, 073501 (2011).